Sensors and Materials, Vol. 35, No. 8 (2023) 2897–2908
MYU Tokyo

S & M 3363

Effects of Annealing Temperature on Optical and Electrical Properties of Different Multilayer Film Structures for Photoelectric Sensors

Tang-Yi Tsai,[1] Chia-Ju Liu,[1] Guan-Lin Guo,[2]
Sheng-Lung Tu,[3] and Tao-Hsing Chen[2*]

[1]Graduate Institute of Science Education and Environmental Education, National Kaohsiung Normal University, No. 116, Heping 1st Rd., Lingya District, Kaohsiung City 80201, Taiwan
[2]Department of Mechanical Engineering, National Kaohsiung University of Science and Technology, Kaohsiung City 807, Taiwan, No. 415, Jiangong Rd., Sanmin Dist., Kaohsiung City 807618, Taiwan
[3]Department of Resources Engineering, National Cheng Kung University, Tainan City 701, Taiwan, No. 1 University Road, Tainan 70101, Taiwan

(Received April 12, 2023; accepted May 29, 2023; online published June 20, 2023)

Keywords: multilayer film, TiO_2/Nb/ITO sensor, TiO_2/Nb/ZnO sensor, optical property, electrical property

In this study, multilayer transparent conductive films were formed by depositing titanium dioxide (TiO_2) and zinc oxide (ZnO) or indium tin oxide (ITO) on a glass substrate by radio-frequency magnetron sputtering using different sputtering parameters, and by depositing niobium (Nb) of 99.99% purity as an intermediate layer between the two oxide layers by DC magnetron sputtering. It was found that the amount of crystals in all the multilayer film structures increases with the annealing temperature, the TiO_2/Nb/ITO (TNI) multilayer film structure has the best electrical properties when annealed at 500 °C, with the resistivity being 9.22×10^{-4} Ω-cm (with the highest average transmittance being 87.85% at the annealing temperature of 300 °C), and the TNI multilayer film structure also has the highest figure of merit (FOM), i.e., $3.88 \times 10^{-3}\ \Omega^{-1}$. However, the TiO_2/Nb/ZnO (TNZ) film annealed at 500 °C had the resistivity of 1.63×10^{-2} Ω-cm, the transmittance of 81.20%, and the FOM of 1.66×10^{-8} Ω^{-1}. The results showed that the TNI multilayer film had the best optical and electrical properties. The results of this study indicate that such multilayer film structures are suitable for use as photoelectric sensors.

1. Introduction

Transparent conductive oxide (TCO) films are photoelectric materials that integrate optical transparency with electrical conductivity.[(1–4)] Such photoelectric materials defy the traditional concept that transparent substances in nature are usually not electrically conductive (e.g., glass), whereas electrically conductive substances in nature are usually opaque (e.g., metal and graphite). TCO films feature a combination of electrical conductivity and transparency and are

*Corresponding author: e-mail: thchen@nkust.edu.tw
https://doi.org/10.18494/SAM4426

ISSN 0914-4935 © MYU K.K.
https://myukk.org/

therefore widely used in a variety of photoelectric devices and sensors such as solar cells, liquid crystal displays, gas detectors, thermally conductive glass for use in airplanes and vehicles, and organic light-emitting devices.[5–8] Common TCO film materials are zinc oxide (ZnO), indium (III) oxide (In_2O_3), titanium dioxide (TiO_2), tin (IV) oxide (SnO_2), and cadmium oxide (CdO), and in order to increase the electrical conductivity and transparency of single-layer TCO films, research and development efforts have been made, leading to the discovery that both the optical and electrical properties of doped single-layer films such as ZnO:Al, SnO_2:Sb, and In_2O_3:Sn (also known as indium tin oxide or ITO) are effectively enhanced.[9–13] However, with the advancement of technology, particularly in the field of microelectronics, the requirements for TCO films have increased. Therefore, researchers proposed to achieve better optical and electrical properties by creating a multilayer film structure analogous to a composite material. Such multilayer film structures mainly include double- and triple-layer structures formed by at least one oxide film and at least one metal film. An oxide/metal/oxide or metal oxide/metal/metal oxide triple-layer film is also referred to as a sandwich film.[14–16] Such films are configured to suppress the reflection of visible light by the intermediate metal layer and thereby achieve relatively high transmittance.[17,18] More specifically, by controlling the refractive indices and optical thicknesses of the upper and lower layers of the sandwich film structure properly, reflection by the intermediate metal layer can be reduced to increase the transmittance of the entire film. Generally, a TCO should have such basic properties as an energy gap larger than 3 eV, a resistance of 10^{-4} to 10^{-5} Ω,[19] the ability to cut off UV light, and relatively high reflectivity in the infrared spectral region. Therefore, ITO, ZnO, and TiO_2 are all good oxide film materials suitable for making photoelectric sensors.

The performance of a TCO film depends on not only the composition of its materials, but also its manufacturing process. Recently, the technologies commonly used to prepare a TCO film have been magnetron sputtering, vacuum evaporation, the sol–gel method, and ion-assisted deposition.[20–24] Magnetron sputtering allows large uniform films to be made and is therefore the most extensively used method in the industry.

In this study, magnetron sputtering was used to deposit TiO_2/Nb/ITO (or TNI for short) and TiO_2/Nb/ZnO (or TNZ for short) sandwich films. Then, we deposited the intermediate metal layer, i.e., the Nb layer between the oxide thin films. To improve the optical and electrical properties, we also utilized the annealing process under different annealing temperatures. Then, a series of tests were conducted on the electrical and optical properties of the sandwich films to identify the multilayer sandwich film structure with the highest quality.

2. Experimental Procedure and Material Preparation

A glass substrate was cut into an appropriate size of 2 × 2 cm^2. The cut glass substrate was washed in alcohol with an ultrasonic vibrator for 10 min and then rinsed with deionized water, before being dried in an oven (100 °C) for 1 h. The sputtering equipment used was a magnetron sputtering system, and the target materials used in the experiment were 99.99% pure TiO_2, ITO, ZnO, and metal Nb. Before film deposition, air was drawn out of the reaction chamber until the pressure in the chamber became lower than 1.0×10^{-3} Pa. Then, a certain amount of Ar/N gas

was introduced into the chamber through a gas flow meter, with the flow rate being 6 sccm. To carry out the deposition process, the sputtering parameters selected for the TiO_2 target material included a power of 100 W, a chamber pressure of 6 mTorr, an Ar flow rate of 15 sccm, and a sputtering time of 90 min. The sputtering parameters selected for the ITO and ZnO target materials included a power of 60 W and a sputtering time of 30 min, and the parameters for the metal Nb target material included a power of 20 W, a chamber pressure of 6 mTorr, an Ar flow rate of 15 sccm, and a sputtering time of 5 min. Once the deposition process was completed, the prepared films were taken out of the reaction chamber and placed in a vacuum annealing furnace to be annealed at 200, 300, 400, or 500 °C. After annealing, the films were kept for 1 h and then allowed to cool to room temperature naturally. The thicknesses of the completed films were measured with an α-step profilometer (KLA-Tencor). The surface topography of the films was observed using an atomic force microscope (Bruker Dimension FastScan - XR), and the crystalline structures of the films were analyzed using an X-ray diffractometer (XRD, SIEMENS D-500). The resistivity, current carrier concentration, and electron mobility of each film were measured using a Hall-effect measuring instrument (AHM-800B). As for the optical properties of the films, optical transmittance was measured using a UV-VIS spectrophotometer (Hitachi 2900).

3. Results and Discussion

3.1 Measurement of film thickness

Table 1 shows the thickness measurements taken with the α-step profilometer of the multilayer film structures formed by sputtering. The annealing process did not change the film thicknesses significantly. The changes were only about 2 nm. (The annealing process caused even less change in the optical and electrical properties of the films, as shown by the corresponding measurements below.)

3.2 Analysis of XRD properties of film

Figures 1 and 2 show the properties of the multilayer film structures with an intermediate dopant (i.e., Nb) layer. The unannealed multilayer films were in an amorphous state, i.e., no crystalline phase was found in those films. The crystalline phase began to present in the TNI films when the annealing temperature was 300 °C. The (222), (400), (411), (431), (440), and (622) peaks were found at 30.5, 35.5, 37.7, 45.9, 51.1, and 61.6°, respectively, but all the peaks correspond to In_2O_3, indicating that Nb ions might have been substituted, and thereby incorporated, into the In_2O_3 lattices, with (222) being the major growth direction. As the

Table 1
Comparison of thicknesses of different multilayer films.

Multilayer	Thickness (nm)
TNI	147.30
TNZ	102.90

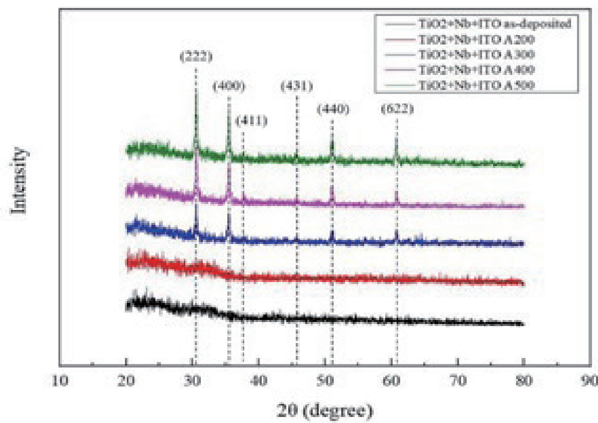

Fig. 1. (Color online) XRD graph of TNI annealed at different temperatures.

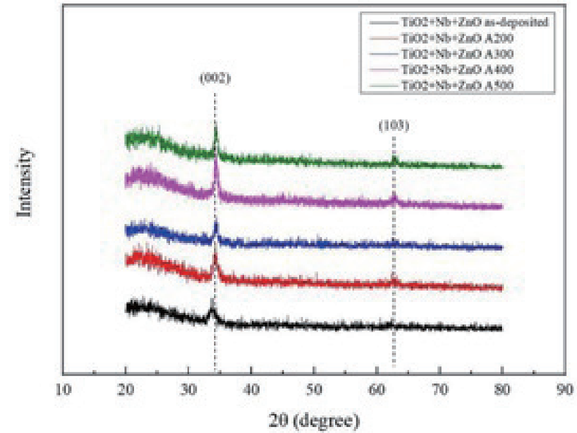

Fig. 2. (Color online) XRD graph of TNZ annealed at different temperatures.

annealing temperature increased, the greatest peak value appeared when the annealing temperature was 500 °C.

The main peak of the TNZ films occurred at 34.3°, with (002) being the major growth direction. The (103) peak appeared at 63.1°. Both peaks correspond to ZnO. As with the TNI films, the peaks were shifted slightly to the right as the annealing temperature increased. Moreover, no peak that corresponds to TiO_2 or Nb_2O_5 was observed, and this indicates that Nb ions had been doped evenly into the TiO_2 and ZnO lattices.

3.3 Comparison of electrical conductivity of films

Tables 2 and 3 show the electrical properties of the multilayer films annealed at different temperatures. As can be seen in the XRD graph of the TNI films, the TNI film annealed at 200

Table 2
Electrical properties of TNI annealed at different temperatures.

TNI: TiO_2 100 W 90 min / Nb 20 W 5 min / ITO 60 W 30 min			
Annealing temperature (°C)	Resistivity (Ω-cm)	Mobility (cm^2/Vs)	Carrier concentration (cm^{-3})
As-deposited	1.51×10^{-3}	2.26×10	5.06×10^{19}
200	2.51×10^{-3}	3.14×10	7.88×10^{19}
300	1.17×10^{-3}	3.73×10	1.05×10^{20}
400	1.06×10^{-3}	4.24×10	2.31×10^{20}
500	9.22×10^{-4}	5.48×10	4.55×10^{20}

Table 3
Electrical properties of TNZ annealed at different temperatures.

TNZ: TiO_2 100 W 90 min / Nb 20 W 5 min / ZnO 60 W 30 min			
Annealing temperature (°C)	Resistivity (Ω-cm)	Mobility (cm^2/Vs)	Carrier concentration (cm^{-3})
As-deposited	4.71×10^{-2}	1.24×10	1.82×10^{18}
200	8.12×10^{-1}	1.60×10	8.79×10^{17}
300	3.67×10^{-2}	2.89×10	3.37×10^{18}
400	3.36×10^{-2}	2.95×10	4.77×10^{18}
500	1.63×10^{-2}	3.62×10	6.75×10^{18}

°C as well as the unannealed one were in an amorphous state, so it can be inferred that the resistivity of the TNI film annealed at 200 °C increased mainly because the crystal grains in the film were still in the growth stage. When the annealing temperature was 300 °C, the resistivity began to decrease. The lowest resistivity, i.e., 9.22×10^{-4} Ω-cm, was obtained when the annealing temperature was 500 °C.

The TNZ film annealed at 500 °C had the lowest resistivity, i.e., 1.63×10^{-3} Ω-cm, mainly because it had the highest current carrier concentration, i.e., 6.75×10^{18} cm^{-3}. As can be seen in the XRD graph of the TNZ films, the highest (002) peak was observed when the annealing temperature was 500 °C, and this indicates that when the annealing temperature was 500 °C, the ZnO structure grew relatively well, with Nb ions diffused evenly into the ZnO and TiO_2 layers such that the resistivity of the film decreased.

3.4 Comparison of optical properties of films

Table 4 and Figs. 3 and 4 show the changes in the energy gap of the multilayer films before and after annealing. The energy gap was calculated using the following equation:[25,26]

$$(\alpha h\upsilon)^2 = A(h\upsilon - Eg), \quad (1)$$

Table 4
Comparison of energy gaps of multilayer films annealed at different temperatures.

	Energy gap (eV)	
Annealing temperature (°C)	TNI	TNZ
As-deposited	3.46	3.26
200	3.37	3.27
300	3.60	3.30
400	3.55	3.33
500	3.56	3.27

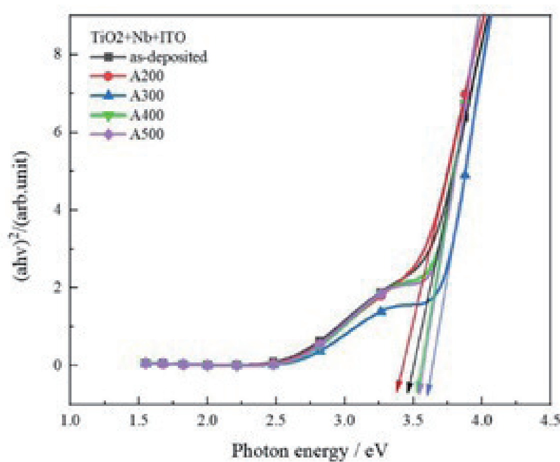

Fig. 3. (Color online) Energy gaps of TNI annealed at different temperatures.

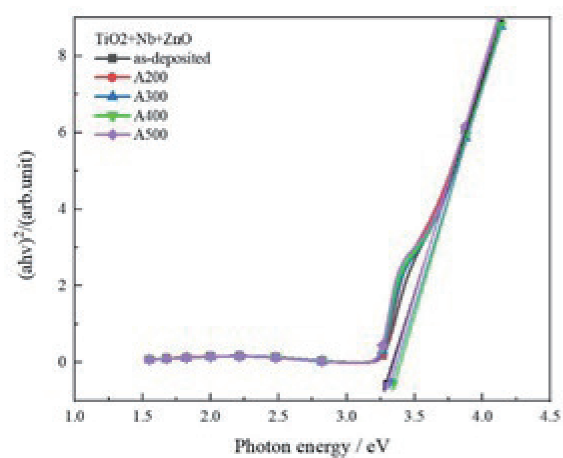

Fig. 4. (Color online) Energy gaps of TNZ annealed at different temperatures.

where A is a constant, and α and $h\upsilon$ are the absorption coefficient and energy of the incident radiation, respectively. It can be seen in Table 4 that the TNI multilayer film structure annealed at 300 °C had the largest energy gap, i.e., 3.60 eV.

The average transmittance of the TNI films (see Fig. 5) was closely related to the current carrier concentration. As the annealing temperature increased, the highest average transmittance, i.e., 87.85%, was obtained when the annealing temperature was 300 °C, which is in line with the trend of the electrical conductivity measurements. When the annealing temperature increased, the metal atoms in the intermediate metal layer were able to be doped into and substitute for the oxide atoms in the upper and lower oxide layers after receiving the energy; as a result, the reflection of visible light by the metal layer was reduced. The energy gap of an ITO increases with increasing current carrier concentration mainly because the Fermi level moves into the conduction band such that an electron needs more energy in order to jump from the valence band to the conduction band (this phenomenon being known as the Burstein–Moss effect). The TNI film annealed at 300 °C had the largest energy gap, i.e., 3.60 eV, and this corresponds to the trend of the electrical property.

The TNZ film annealed at 500 °C had the highest average transmittance, i.e., 81.20% (see Fig. 6), and this was mainly because when the annealing temperature increased, metal atoms in the metal layer were able to be doped into and substituted for the oxide atoms in the upper and lower oxide layers after receiving the energy, thereby reducing the reflection of visible light by the metal layer and consequently increasing the average transmittance.[27] According to the energy gap values, the TNZ film annealed at 400 °C had the largest energy gap, i.e., 3.33 eV, which satisfies the requirement for a wide-band-gap semiconductor.

3.5 Analysis of figures of merit (FOM)

As far as transparent conductive films are concerned, the quality of the film material can be expressed by the FOM to facilitate comparison, wherein the FOM is calculated from resistivity

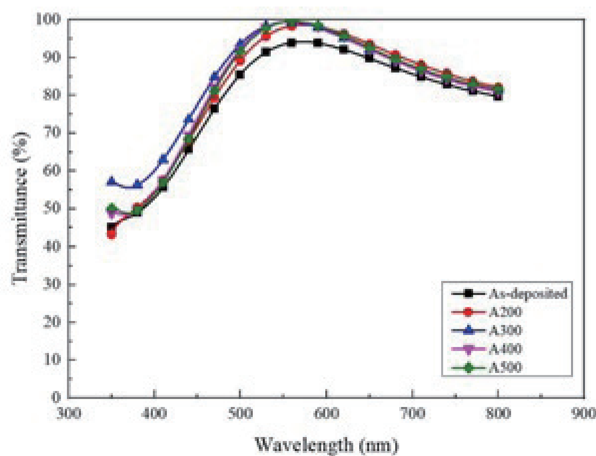

Fig. 5. (Color online) Transmittance of TNI annealed at different temperatures.

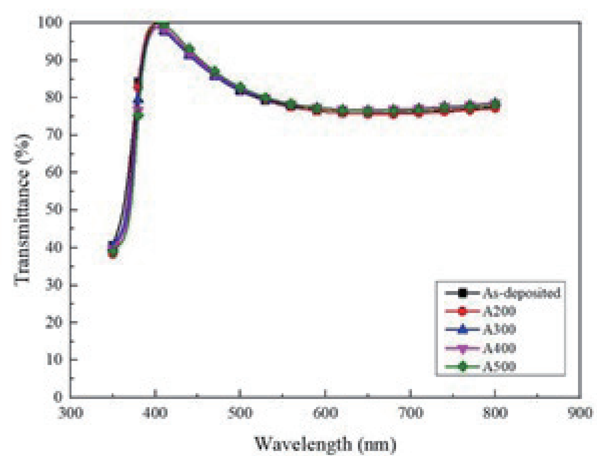

Fig. 6. (Color online) Transmittance of TNZ annealed at different temperatures.

and transmittance.[28,29] As can be known from the equation below, the FOM is directly proportional to transmittance to the power of 10. Transmittance, therefore, is a critical factor in the FOMs of such films. A high FOM requires relatively low resistivity and high transmittance.

$$\Phi_{TC} = \frac{T_{av}^{10}}{R_{sh}} \tag{2}$$

Table 5 shows the FOMs of the TNI and TNZ films annealed at different temperatures. According to Table 5, the TNI film annealed at 500 °C had the highest FOM, i.e., 3.88×10^{-3} Ω^{-1}. As the optical transmittance of the TNI films did not change much with increasing annealing temperature (see Fig. 5), it can be inferred that resistivity was the key factor of the FOM. Because the lowest resistivity was obtained when the annealing temperature was 500 °C, the highest FOM was obtained when the annealing temperature was 500 °C.

In the case of the TNZ films, the film annealed at 500 °C also had the highest FOM, i.e., 1.66×10^{-8} Ω^{-1}. As the optical transmittance of the TNZ films did not change much with the annealing temperature (see Fig. 6), it can be inferred that resistivity was also the key factor of the FOM. The lowest resistivity was also obtained when the annealing temperature was 500 °C, so the highest FOM was obtained when the annealing temperature was 500 °C

3.6 Analysis of surface feature

In this study, a surface topography analysis, or roughness analysis, was performed on the films before and after annealing using an atomic force microscope (AFM). The analysis results are summarized in Table 6, which shows the surface roughness (Ra) values. All the TNI multilayer film structures had Ra values of less than 1 nm, indicating that those multilayer films

Table 5
FOMs of multilayer films annealed at different temperatures.

	FOM Φ_{TC} (Ω^{-1})	
Annealing temperature (°C)	TNI	TNZ
As-deposited	2.13×10^{-3}	8.41×10^{-10}
200	1.40×10^{-3}	2.42×10^{-9}
300	2.15×10^{-3}	1.73×10^{-9}
400	2.27×10^{-3}	1.35×10^{-9}
500	3.88×10^{-3}	1.66×10^{-8}

Table 6
Surface roughness values of different multilayer film structures.

Annealing temperature (°C)	TNI Ra (pm)	TNZ Ra (pm)
As-deposited	8.51	25.9
200	7.41	22.2
300	6.97	14.2
400	6.81	13.2
500	6.48	12.2

had very flat surfaces. The Ra value was reduced when the annealing temperature increased, indicating that the annealing process helped improve the surface roughness of the films. All the ITO films had smooth, continuous surfaces. The same phenomenon (roughness reduced when the annealing temperature increased) was also found in multilayer films whose third layer was ZnO. Figures 7 and 8 are AFM images showing the surface conditions of different multilayer

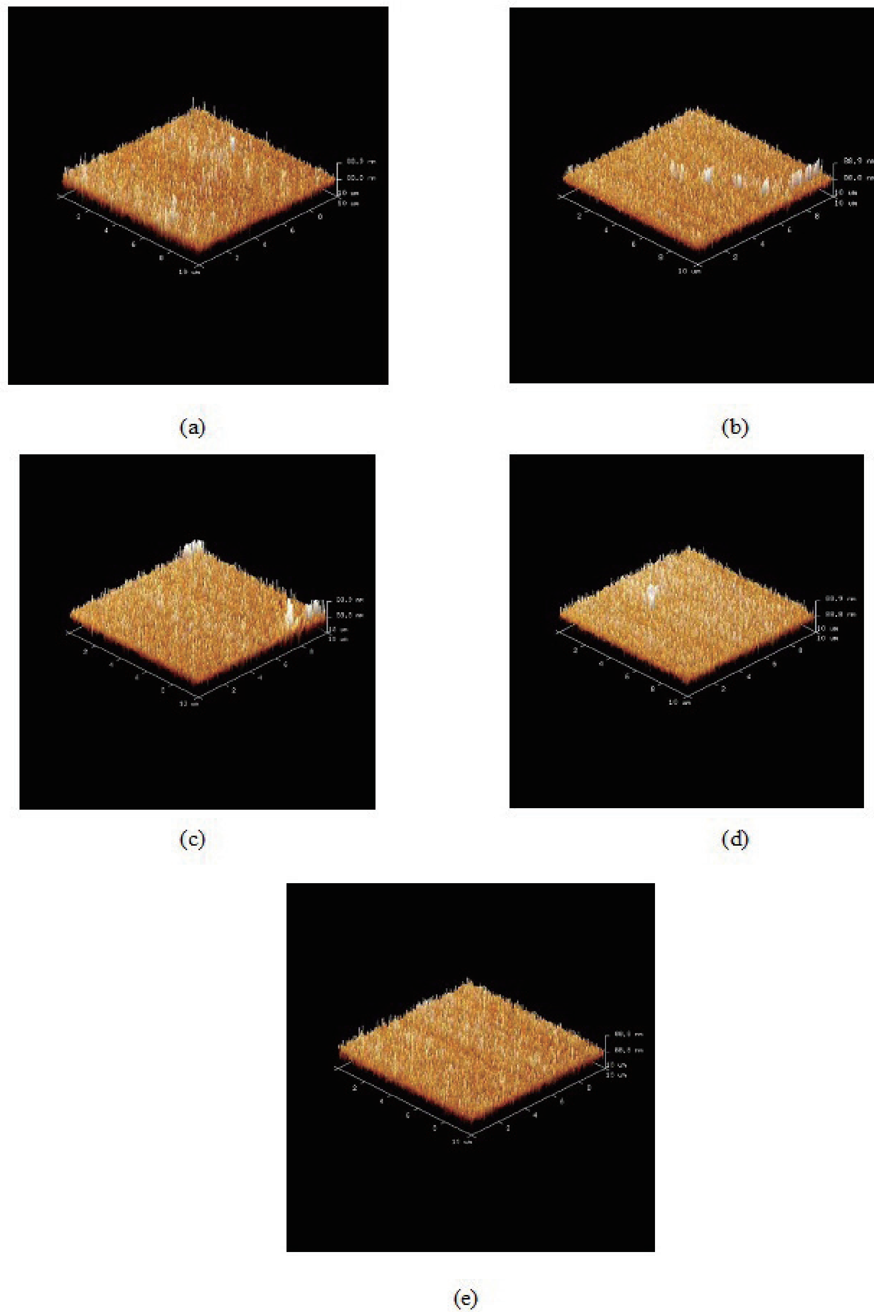

Fig. 7. (Color online) Surface features of (a) as-deposited TNI multilayer film structure and those annealed at (b) 200, (c) 300, (d) 400, and (e) 500 °C.

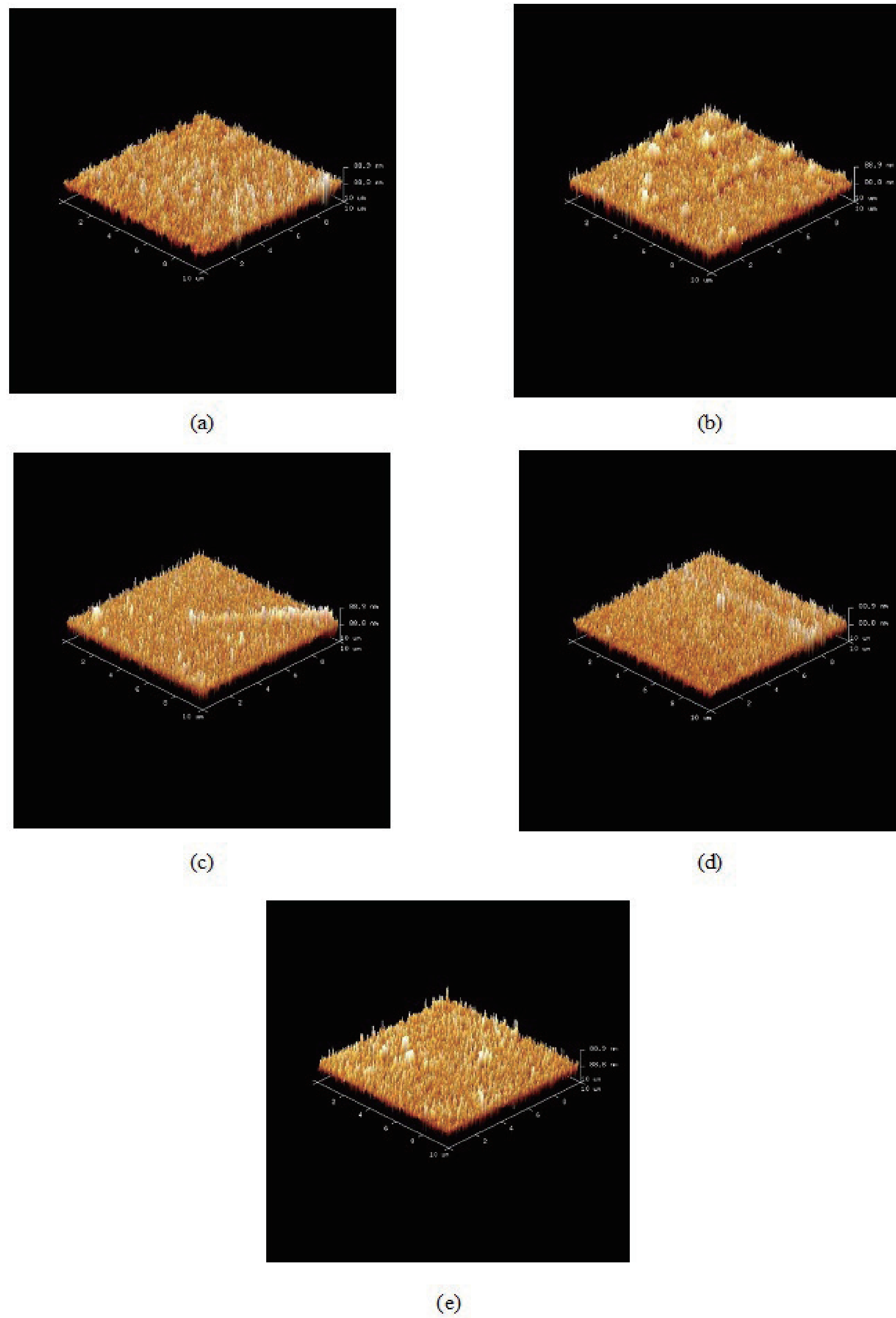

Fig. 8. (Color online) Surface features of (a) as-deposited TNZ multilayer film structure and those annealed at (b) 200, (c) 300, (d) 400, and (e) 500 °C.

film structures. As can be seen in the figures, the deposited surface layers of both types of multilayer film structure were even and had a dense texture.

4. Conclusions

According to the experimental results, the overall thicknesses of the TNI multilayer films barely changed under different annealing temperatures. As to the XRD structural properties, the unannealed TNI film and the TNI film annealed at 200 °C were both in an amorphous state, and the crystalline phase began to show when the annealing temperature was 300 °C. With regard to electrical properties, the resistivity of the TNI films was increased when "no annealing" was changed to "annealing at 200 °C" and this was mainly because the crystal grains in those films were still in the growth stage. Resistivity began to decrease when the annealing temperature was 300 °C, and the lowest resistivity, i.e., 9.22×10^{-4} Ω-cm, was obtained when the annealing temperature was 500 °C. When it comes to optical transmittance, the highest average transmittance of the TNI films, i.e., 87.85%, was obtained when the annealing temperature was 300 °C. The largest energy gap, i.e., 3.60 eV, was also obtained when the annealing temperature was 300 °C. As for surface topography, the AFM images of the TNI films show that the Ra values of the annealed films as well as the unannealed one were less than 1 nm and that the Ra value was reduced when the annealing temperature increased, indicating that the annealing process helped improve the surface roughness of the films and contributed to high flatness. Last but not least, the TNZ film annealed at 500 °C had the highest FOM, i.e., 1.66×10^{-8} Ω^{-1}, and this was because the lowest resistivity was obtained when the annealing temperature was 500 °C. It can be considered that the two multilayer thin films are suitable for photosensor applications.

Acknowledgments

This study is supported by Project Nos. MOST 110-2628-E-992-002 and 111-2628-E-992-001 MY2 of the Ministry of Science and Technology. The authors would like to thank the Ministry of Science and Technology for their support. The authors gratefully acknowledge the use of XRD2 of NSTC 111-2731-M-006-001 belonging to the Core Facility Center of National Cheng Kung University.

References

1 T. H. Chen, T. C. Cheng, and Z. R. Hu: Microsyst. Technol. **19** (2013) 1787. https://doi.org/10.1007/s00542-013-1837-5
2 C. F. Liu, T. H. Chen, and J. T. Huang: Sens. Mater. **32** (2020) 3727. https://doi.org/10.18494/SAM.2020.3138
3 P. Nunes, E. Fortunato, P. Tonello, F. B. Fernandes, P. Vilarinhom, and R Martins: Vacuum **64** (2002) 281. https://doi.org/10.1016/S0042-207X(01)00322-0
4 T. Minami: Thin Solid Films **516** (2008) 1314. https://doi.org/10.1016/j.tsf.2007.03.082
5 P. K. Nayak, J. Yang, J. Kim, S. Chung, J. Jeong, C. Lee, and Y. Hong: J. Phys. D: Appl. Phys. **42** (2008) 035102. https://doi.org/10.1088/0022-3727/42/3/035102
6 H. S. Das, R. Das, P. K. Nandi, S. Biring, and S. K. Maity: Appl. Phys. A **127** (2021) 225. https://doi.org/10.1007/s00339-021-04339-6
7 E. Nam, Y. H. Kang, D. Jung, and Y. S. Kim: Thin Solid Films **518** (2010) 6245. https://doi.org/10.1016/j.tsf.2010.02.068
8 A. Eshaghi and M. Hajkarimi: Optik **125** (2014) 5746. https://doi.org/10.1016/j.ijleo.2014.07.056Get rights and content

9 S. U. Park and J. H. Koh: Ceram. Int. **40** (2014) 10021. https://doi.org/10.1016/j.ceramint.2014.02.101
10 T. H. Chen and C. L. Yang: Opt. Quantum Electron. **48** (2016) 533. https://doi.org/10.1007/s11082-016-0808-3
11 T. H. Chen and T. Y. Chen: Nanomaterials **5** (2015) 1831. https://doi.org/10.3390/nano5041831
12 M. Y. Yen, T. H. Chen, P. H. Lai, S. L. Tu, and Y. H Shen: Sens. Mater. **33** (2021) 3941. https://doi.org/10.18494/SAM.2021.3706
13 W. S. Liu, W. T. Hsieh, S. Y. Chen, and C. S. Huang: Sol. Energy **174** (2018) 83. https://doi.org/10.1016/j.solener.2018.08.050.
14 T. H. Chen and H. T. Su: Sens. Mater. **30** (2018) 2541. https://doi.org/10.18494/SAM.2018.2056
15 D. Kaya, M. Akyol, E. Ş. Tüzemen, and A. Ekicibil: Optik **265** (2022) 169595. https://doi.org/10.1016/j.ijleo.2022.169595
16 J. H. Kim, Y. J. Moon, S. K. Kim, Y. Z. Yoo, and T. Y. Seong: Ceram. Int. **41** (2015) 14805. https://doi.org/10.1016/j.ceramint.2015.08.001
17 J. C. Fan, F. J. Bachner, G. H. Foley, and P. M. Zavracky: Appl. Phys. Lett. **25** (1974) 693. https://doi.org/10.1063/1.1655364
18 A. Dhar and T. L. Alford: APL Mater. **1** (2013) 012102. https://doi.org/10.1063/1.4808438
19 S. Calnan and A. N. Tiwari: Thin Solid Films **518** (2013) 1839. https://doi.org/10.1016/j.tsf.2009.09.044
20 P. Nunes, D. Costa, E. Fortunato, and R. Martins: Vacuum **64** (2002) 293. https://doi.org/10.1016/S0042-207X(01)00323-2
21 T. Minami, S. Ida, T. Miyata, and Y. Minamino: Thin Solid Films **445** (2003) 268. https://doi.org/10.1016/S0040-6090(03)01159-3
22 M. C. Jun and J. H. Koh: J. Nanosci. Nanotechnol. **13** (2013) 1403. https://doi.org/10.1166/jnn.2013.7314
23 M. S. Farhan, E. Zalnezhad, A. R. Bushroa, and A. D. Sarhan: Int. J. Precis. Eng. Manuf. **14** (2013) 1465. https://doi.org/10.1007/s12541-013-0197-5
24 C. F. Liu, S. C. Shi, T. H. Chen, and G. L. Guo: Sens. Mater. **34** (2022) 4127. https://doi.org/10.18494/SAM4133
25 T. Wang, Y. Liu, Q. Fang, M. Wu, X. Sun, and F. Lu: Appl. Surf. Sci. **257** (2011) 2341. https://doi.org/10.1016/j.apsusc.2010.09.100Get rights and content
26 A. A. Yadav, E. U. Masumdar, A. V. Moholkar, M. Neumann-Spallart, K. Y. Rajpure, and C. H. Bhosale: J. Alloys Compd. **488** (2009) 350. https://doi.org/10.1016/j.jallcom.2009.08.130
27 C. F. Liu, T. H. Chen, and Y. S. Huang: Sens. Mater. **32** (2021) 2321. https://doi.org/10.18494/SAM.2020.2867
28 S. A. Knickerbocker and A. K. Kulkarni: J. Vac. Sci. Technol., A **13** (1995) 1048. https://doi.org/10.1116/1.579583
29 B. Sarma, D. Barman, and B. K. Sarma: Appl. Surf. Sci. **479** (2019) 786. https://doi.org/10.1016/j.apsusc.2019.02.146

About the Authors

Tang-Yi Tsai received his M.S. degree from the Graduate Institute of Science Education and Environmental Education, IEMBA, National Kaohsiung Normal University, Taiwan, in 2008. He is now a Ph.D. candidate of the Graduate Institute of Science Education and Environmental Education. His research interests are in environment engineering, environmental education, and environmental sensors. (vida.king@msa.hinet.net)

Chia-Ju Liu received her Ph.D. degree from the Graduate Institute of Science Education, National Taiwan Normal University, Taiwan, in 1999. She is now a professor at the Graduate Institute of Science Education and Environment, National Kaohsiung Normal University. Her research interests are in science education and optical sensors. (chiaju.nknu@gmail.com)

Guan-Lin Guo received his B.S. degree from National Kaohsiung University of Science and Technology, Taiwan, where he is currently studying toward his M.S. degree. His research interests are in MEMS, materials engineering, and sensors.

Sheng-Lung Tu received his M.S. degree from the Department of Mechanical Engineering, National Cheng Kung University, in 2010 and his Ph.D. degree from the Department of Resources Engineering, National Cheng Kung University, in 2014. Since 2014, he has been working as a general affairs officer at National Cheng Kung University. His research interests are in PVD technology, thin film technology, and sensors.

Tao-Hsing Chen received his B.S. degree from National Cheng Kung University, Taiwan, in 1999 and his M.S. and Ph.D. degrees from the Department of Mechanical Engineering, National Cheng Kung University, in 2001 and 2008, respectively. From August 2008 to July 2010, he was a postdoctoral researcher at the Center for Micro/Nano Science and Technology, National Cheng Kung University. In August 2010, he became an assistant professor at National Kaohsiung University of Applied Sciences (renamed National Kaohsiung University of Science and Technology), Taiwan. Since 2016, he has been a professor at National Kaohsiung University of Science and Technology. His research interests are in metal materials, TCO thin films, thermal sensors, and photosensors. (thchen@nkust.edu.tw)